Journal of Volcanology and Geothermal Research
November 2020, Volume 406, Pages 107046 (7p.)
https://doi.org/10.1016/j.jvolgeores.2020.107046
https://archimer.ifremer.fr/doc/00649/76113/

Mapping the geometry of volcanic systems with magnetotelluric soundings: Results from a land and marine magnetotelluric survey performed during the 2018–2019 Mayotte seismovolcanic crisis

Darnet M. [1, *], Wawrzyniak P. [1], Tarits Pascal [2, 3, 4], Hautot S. [3], D'Eu J.F. [4]

[1] BRGM, Bureau des Recherches Géologiques et Minières, 3 av. Claude-Guillemin, BP 36009, 45060 Orléans Cedex 2, France
[2] IUEM, Institut Universitaire Européen de la Mer, LGO, UMR 6538 - IUEM/UBO, Place Nicolas Copernic, Plouzané, 29280, France
[3] IMAGIR Sarl, Tech-Iroise, ZA de Mespaol 2, 1 rue des Ateliers, 29290 Saint Renan,France
[4] MAPPEM Geophysics SAS, Marine Electromagnetic Investigation, Batiment Tech-Iroise, 1 rue des Ateliers, Zone de Mespaol, 29290 Saint-Renan, France

* Corresponding author : M. Darnet, email address : m.darnet@brgm.fr

p.wawrzyniak@brgm.fr ; pascal.tarits@univ-brest.fr ; sophie.hautot@imagir.eu ; jf.deu@mappem-geophysics.com

Abstract :

A major seismovolcanic crisis has afflicted the islands of Mayotte, Comoros Archipelago, since May 2018, although the origin is debated. Magnetotellurics (MT), which is sensitive to hydrothermal and/or magmatic fluids and can map the subsurface electrical resistivity structure, can provide insight by revealing the internal structure of the volcanic system. In this paper, we report the results of a preliminary land and shallow marine MT survey performed on and offshore the island nearest the crisis. The 3D inversion-derived electrical resistivity model suggests that the island is underlain by a shallow ~500-m-thick conductive layer atop a deeper, more resistive layer, possibly associated with a high-temperature geothermal system. At depths of ~15 km, the resistivity drops by almost two orders of magnitude, possibly due to partial melting. Further petrophysical and geophysical studies are underway for confirmation and to map the geometry and evolution of the volcanic system.

Highlights

► A major seismovolcanic crisis has afflicted the islands of Mayotte, Comoros Archipelago, since May 2018, although the origin is debated. ► We report the results of a preliminary land and shallow marine MT survey performed on and offshore the island nearest the crisis. ► The 3D inversion-derived electrical resistivity model suggests that the island is underlain by a shallow ~500-m-thick conductive layer atop a deeper, more resistive layer, possibly associated with a high-temperature geothermal system. ► At depths of ~15 km, the resistivity drops by almost two orders of magnitude, possibly due to partial melting.

Keywords : magnetotelluric, electrical resistivity, seismovolcanic, geothermal

1. Introduction

Mayotte, located along a WNW-ESE oceanic ridge at the boundary of the Lwandle and Somalian plates, represents a region of islands within the volcanic Comoros Archipelago north of the Mozambique Channel between the northern tip of Madagascar and the eastern coast of Mozambique. The region of Mayotte is composed predominantly of two main islands, namely, Grande Terre (363 km^2) to the west and Petite Terre (11 km^2) to the east (figure 1).

In May 2018, an offshore seismovolcanic crisis initiated approximately 50 km to the east of Mayotte; the crisis included the largest seismic event ever recorded in the Comoros with a Mw=5.9 (Lemoine et al., 2019; Cesca et al., 2020), and an estimated 5 km^3 of lava was released from an eruptive site in the same area (REVOSIMA bulletin, http://www.ipgp.fr/fr/actualites-reseau). The seismicity subsequently migrated to the west and is now located between 5 and 15 km from the Petite Terre (figure 1). The possible causes of the Comoros volcanism continue to constitute a topic of controversy (Lemoine et al., 2019), as its origin could be related to i) the presence of a hot spot (Emerick and Duncan, 1982), ii) lithospheric fractures (Nougier et al., 1986), or iii) a combination of the two, i.e., regional extension in conjunction with asthenospheric processes (Debeuf, 2004; Michon, 2016). Forecasts regarding the evolution of this crisis remain very uncertain and require the gathering of additional geoscientific data, particularly geophysical data, to help understand the internal structure of the corresponding volcanic system.

Magnetotellurics (MT) is a geophysical method commonly used to generate electrical resistivity images of the subsurface. By combining long-period (>1 s) fluctuations of natural electric and magnetic fields, MT analysis can infer the electrical resistivity structure of the Earth at depths reaching several tens of kilometers (Chave and Jones, 2012). However, this technique suffers one major drawback: its sensitivity to anthropic noise, which can obfuscate signals of interest (Junge, 1996). Accordingly, robust data processing methods have been developed to reduce the influence of such noise (Chave and Thomson, 2004; Egbert, 2002).

At temperatures lower than <500-800°C, the electrical resistivity of saturated volcanic rock depends strongly on the physical and chemical properties of the fluid filling the pore space and on the presence of alteration minerals (Revil et al., 1998; Nono et al., 2018). At higher temperatures, intramineral conduction mechanisms dominate, and upon reaching the solidus temperature, the presence of melt significantly influences the rock electrical resistivity (Laumonier et al., 2017). Therefore, measurements of electrical resistivity can help assess the presence of

hydrothermal and/or magmatic fluids. This sensitivity explains why MT is commonly used in geothermal exploration (Spichak and Manzella, 2009) and volcano imaging (Ingham et al., 2009). MT has also recently been applied to monitor resistivity changes in volcanoes (Aizawa et al., 2013; Wawrzyniak et al., 2017; Ladanivskyy et al., 2018). However, the application of time-lapse MT continues to be challenging due to variations in geomagnetic activity, sources of anthropic noise and the stability of the MT setup (Abdelfettah et al., 2018).

In this paper, we present the results of an land and shallow marine MT survey carried out during the seismovolcanic crisis of Mayotte. The main challenge associated with performing MT measurements on this island was the presence of strong anthropic noise and the small size of the island; accordingly, both land and shallow marine data had to be acquired. The data quality was ultimately good over a wide period range (from 0.01s to 1000s), providing the opportunity to characterize the deep (> 10 km) electrical resistivity structure of the island. After describing the MT field setup, we present the processed MT data and the results from a 3D inversion. Furthermore, we discuss both the quality of the data with a time-lapse MT analysis and the resolution of the resistivity model with a sensitivity study. Finally, we conclude with a discussion of possible explanations for the observed electrical resistivity anomalies.

2. MT data acquisition and processing

2.1. Land MT survey

Due to its high degree of urbanization (e.g., airports, power plants, military bases), Petite Terre island presents a challenging environment in which to perform passive electromagnetic (EM) measurements. To mitigate the impacts of ambient EM noise on the MT soundings, we deployed two MT stations on the most isolated parts of the island (sites L1 and L2) and one remote reference MT station on Grande Terre island (site L0), approximately 15 km away from Petite Terre (figure 1). We used ADU07 systems (Metronix, Germany) with unpolarizable $Pb-PbCl_2$ electrodes (Wolf Ltd, Hungary) and MSF07 magnetic coils (Metronix, Germany). The sensors were oriented toward the north and east (x=north, y=east). MT recordings were performed synchronously for 4 days at both sites.

We processed the time series following the robust approach of Chave and Thomson (2004) with a remote reference MT station. We computed the full impedance tensor at each site at periods

ranging from 0.001 to 1000 s. An MT sounding example is shown in figure 2. Overall, the data were of good quality over the period range; however, at 1-10 s, noise could not be excluded due to the weakness of the primary field. The phase tensor ellipses shown in figure 1 were extracted from the phase tensors calculated using the formula of Booker (2014).

2.2. Marine MT survey

Because of the limited number of sites favorable for MT measurements on Petite Terre island, we deployed four new-generation low-power shallow marine MT systems (STATEM) around the island at water depths ranging from 15 to 25 m (figure 1). These STATEM systems were recently developed by MAPPEM Geophysics and the Ocean Geosciences Laboratory (LGO), European Institute for Marine Studies (IUEM). Each STATEM system records the two horizontal components of the electric field with 5m-long electric dipoles and marine $Ag - AgCl$ electrodes. The three components of the magnetic field were obtained from a 3-component fluxgate sensor. With an optimized datalogger, the measurements were performed synchronously with the land stations for 2 days at a sampling rate of 512 Hz. The design of the system is such that motion of the system induced by oceanic current is minimized. During the survey, bidirectional tiltmeter measurements performed every second showed that motion and drift of the sensor were minimum (less than +/- 0.2 deg).

Similarly to the land case, the time series were robustly processed with the bounded influence, remote reference processing (BIRRP) code of Chave and Thomson (2004). The processing of shallow marine MT data is a challenging task due to the high level of ocean-induced EM noise that can mask the MT signal. For the electric field, noise can be generated not only by the movement of the water layer (e.g., waves, swells, tides) within the Earth's magnetic field but also by the current-induced motion of the electrodes. Similarly, magnetic field measurements can become contaminated by noise associated with not only ocean-induced electric currents but also the motion of the sensor. As a consequence, both electric and magnetic measurements may exhibit high levels of ocean-induced EM noise that is well correlated and difficult to distinguish from the MT signal. Therefore, the use of a land remote reference is of paramount importance to reduce the impacts of ocean-induced noise (figure S1). Remote referencing between marine sites was sufficient at long periods (> 100 s); hence, the challenge was to obtain the MT impedance at the shortest possible period (< 0.1 s). Depending on the type of noise, magnetic and/or electric field

measurements from the remote reference were used to filter out oceanic noise. An example of the MT transfer function is shown in figure 2. Despite the lack of high-frequency measurements (< 0.01 s) due to the weakness of the MT signals recorded beneath $\sim$ 20 m of seawater, the MT transfer function was reliably recovered over the 0.02 - 1000 s period band and was consistent with the nearby land site (site L2) (figure 2). Nevertheless, similar to the land data, the MT impedance results at 1-10 s were not reliable, as this period range is further impacted by a high level of swell-induced noise.

2.3. Permanent land MT monitoring

Given the good quality of the MT recordings at site L2, the setup was adapted to perform long-term monitoring of the MT impedance tensor (e.g., the cables and recording device were buried). The objective was to to test the feasibility of recording possible resistivity changes at depth related to the seismovolcanic crisis. Permanent measurements of the horizontal components of the electric and magnetic fields began on May 22, 2019. Every four days, the impedance tensor was computed for a comparison with the initial MT results. The time-lapse MT data were processed with a in-house developed open-source Python library (Smai and Wawrzyniak, 2020) using the bounded influence processing method of Chave and Thomson (2004) in a two-stage remote reference configuration.

The time-lapse MT impedance results from May 29^{th} to June 28^{th} are presented in figure 3. We observed that the Kp geomagnetic index (https://www.swpc.noaa.gov/products/planetary-k-index) strongly varied during this period (figure 3a). The most continuous MT soundings (apparent resistivity, phase and phase tensor diagrams) were obtained for the four-day intervals beginning on May 29^{th} and June 12^{th}, when the Kp index remained high (figure 3b and c). Unfortunately, site L2 is located in a relatively dry area of Mayotte, and the ground surrounding the electrodes became progressively dessicated. As a consequence, after June 12, the apparent resistivity and phase tensor estimates became increasingly noisy in the 1 to 5s period range and occasionally at longer periods. These observations illustrate the challenge of performing continuous MT measurements due to the variability of the Earth's magnetic field and local variations in the degree of coupling of the electrodes. Nevertheless, when the Kp index was large and the electrical coupling was good, the MT tensor estimates at long periods (> 100s) were consistent from one 4-day time window to the

other (e.g., between May 29 and June 12). This stability confirms the robustness of the initial MT tensor estimates illustrated in figure 2 as well as the phase tensor parameter estimates.

Long-period MT phase tensor analysis may be implemented to assess the azimuthal variation of the electrical resistivity of a deep regional structure (Booker, 2014). In Mayotte, at a period of approximately 1000 s, the strikes of the phase tensors were approximately N35° at site L0 and N41° at site L2 (figure 1). This indicates that the deep regional structures in Mayotte are electrically more conductive at orientations of N125° at site L0 and N131° at site L2; remarkably, these orientations are roughly the same azimuth as the oceanic ridge (Audru et al., 2010).

3. MT inversion results

The data recorded at the two land and the four marine MT sites were jointly inverted to image the electrical resistivity structure beneath Petite Terre island. We inverted the four components of the MT impedance tensors at all available periods; the period range for the land MT data was 0.009-1000 s, and that for the marine MT data was 0.02-1000 s. We excluded data with large errors, especially within the dead band. For the 3D inversion, we used the MININ3D code from Hautot et al. (2000, 2007). Given the small number of sites, we used a grid of 21x18x18 cells which included the bathymetry of the study area. The total volume of the 3D model was 21x20x13 km^3. The horizontal dimensions of the cells in the central part of the model is 500 x 500 m. The thickness of the layers increased from 5 to 5000 m. The 3D model topped a 1D model with three layers with thicknesses of 13, 58 and 88 km, whose resistivities were also included in the inversion. Except for the marine part (0.3 Ohm.m), the starting model was homogeneous (18 Ohm.m). The 3D inversion was applied to minimize a misfit function between the observed data and the 3D model response at all sites and frequencies weighted by the data variance. Data were the four complex components of the MT tensor. The starting RMS was 9.3, and the RMS decreased down to 2.2.

A cross-section through the shallow (until 5km depth) and deep (until 50km depth) section of the 3D resistivity model is shown in figure S2 and figure 4, respectively. The most prominent feature is the presence of a deep conductive layer (with a resistivity of less than 2 Ohm.m) beneath a depth of 13 km (labelled C1 on figure 4). A shallow conductive layer (resistivity of less than 5 Ohm.m) is also present within the first 500 m of the model (labelled C3 on figure S2). Between

these two conductive structures, the resistivity increases up to $\sim$ 100 Ohm.m. Toward the southeast, the resistivity in the 5-13 km depth range decreases to less than 10 Ohm.m (labelled C2 on figure 4); this conductor is located close to the hypocenters of the seismic events recorded during the seismovolcanic crisis.

To assess the uncertainties in the deep resistivity structures identified in the 3D resistivity model, we performed a sensitivity analysis on both the resistivity of the conductive layer (below a depth of 13 km) and the depth to the top of this conductor (figure 5). The misfit rapidly increases with increasing resistivity below a depth of 13 km, confirming that a conductor of less than 4 Ohm.m is required to fit the data (figure 5a). The optimum depth of this conductor was found at approximately 16 km (figure 5b). However, the misfit increases slowly between this interval indicating that this depth is not very well resolved. We also tested the sensitivity of the model to the presence of the C2 conductor between depths of 5 and 13 km to the southeast of Petite Terre and on the edge of the MT network (figure 4). The absence of this conductor significantly increased the misfit (figure 5c), suggesting that this feature was not an artifact of the inversion process and was constrained by the MT data.

4. Discussion

In this section, we discuss the electrical resistivity structure of the Petite Terre island derived from the inversion of the MT data and propose an interpretation of the geoelectric structure of the island (figure 6).

The presence of a shallow conductive layer overlying a more resistive body beneath the surface of Petite Terre (labelled C3 in figure S2) is consistent with the electrical resistivity structure typically observed under volcanoes exhibiting well-developed hydrothermal systems (Flóvenz et al., 2005; Ussher et al., 2000). According to these models, this shallow conductive layer (resistivity of 1-10 Ohm.m) corresponds to a smectite-rich, low-temperature ($< 220°C$), hydrothermally altered layer, often called a clay cap. For Petite Terre, this layer would be approximately 500 m thick. At greater depth and with increasing temperature ($> 220°C$), the material is less rich in smectite, whereas the illite content increases. Furthermore, porosity tends to decrease with depth, which reinforces the modeled resistivity increase due to the change in alteration products (Ussher et al., 2000) with resistivity values ranging from 20 to 100 Ohm.m. On

Petite Terre, such values are observed below depths of 500 m and deeper and could correspond to a high-temperature geothermal reservoir.

At depths of 13-16 km, the resistivity drops by almost two orders of magnitude, reaching values of a few Ohm-meters (labelled C1 on figure 4). At such depths, the temperature is very likely to exceed 450 °C, which is the estimated temperature at a depth of 15 km for a normal geothermal gradient of 30°C/km (Saemundsson et al., 2009). The electrical signature of rocks under such high-temperature conditions is still not fully understood, but recent laboratory experiments (Kummerow and Raab, 2015b,a; Nono et al., 2018) have shown that at 25-350°C, the resistivity of altered volcanic rock decreases as a result of both increasing surface and electrolytic conduction. Then, under supercritical conditions, i.e., at temperatures of 400-600°C, the electrical resistivity strongly increases due to the evolution of the water density and dielectric constant, which affect both surface and electrolytic conduction. At higher temperatures (> 600°C), mineral conduction dominates the resistivity of the rock; at these temperatures, ferromagnesian minerals serve as the principal contributors of mineral conduction, resulting in a decrease in the rock resistivity. At even higher temperatures (> 1000°C), partial melting may occur, thereby decreasing the rock resistivity further (Laumonier et al., 2017). The low resistivities (a few Ohm-meters) observed throughout Petite Terre at depths of 13-16 km could therefore be caused either by the presence of altered rocks saturated with fluid below the supercritical point (< 400°C) or by the presence of a small fraction of connected melt. At these depths, the temperature exceeds the supercritical point; hence, the most likely explanation for the observed conductive layer is the presence of melt. Similar observations have been reported beneath oceanic ridges on the basis of MT soundings (Baba et al., 2006) and interpreted as being indicative of the presence of melt (Laumonier et al., 2017). This hypothesis is further supported by the good correlation between the electrical strike of the observed phase tensors (figure 1) and the azimuth of the oceanic ridge (Audru et al., 2010). Nevertheless, additional laboratory data (e.g., electrical resistivity measurements on Mayotte volcanic rock samples) and geophysical observations (e.g., imaging of zones characterized by low seismic velocities) are necessary to confirm this interpretation.

Finally, we noticed the presence of a conductive structure in the 5-15 km depth range to the southeast of Petite Terre (labelled C2 on figure 4) close to the seismic events recorded between May 2018 and May 2019. In this area, recent volcanic material and gas emissions have been observed on the seafloor (REVOSIMA bulletins, www.ipgp.fr/fr/actualites-reseau). Accordingly,

this conductive anomaly could be related to recent seismovolcanic activity. Additional deep marine MT sites are currently being deployed in this area to obtain more insight into the presence and geometry of this conductive anomaly and its relationship with the regional seismovolcanic activity. Furthermore, the two permanent land stations at sites L0 and L2 are currently being maintained to perform robust-processing of the deep marine MT sites but also long-term monitoring of any resistivity changes at depth related to the evolution of the seismovolcanic crisis.

5. Conclusions

Since May 2018, a major seismovolcanic crisis has affected the island's of Mayotte in the Comoros Archipelago, providing a unique opportunity to monitor the development of an active volcanic system. Preliminary MT data acquired on and near this island were implemented to image the electrical resistivity structure of the volcanic system. The resulting model suggests the presence of hydrothermal fluids in the shallow part of the system (< 2 km) and magmatic fluids at greater depth (> 15 km). Further petrophysical and geophysical studies (e.g. additional land and offshore MT surveys, seismic surveys) are ongoing to confirm the origin and geometry of these deep conductors and to help better understand the associated magmatic and volcanic activity. In addition, the permanent land MT stations are currently being maintained to perform long-term monitoring of any resistivity changes at depth related to the evolution of the seismovolcanic crisis.

Acknowledgments

We would like to thank the Mayotte branch of the Environment and Energy Management Agency (ADEME) and the General Directorate for Risk Prevention (DGPR) for financially supporting the geophysical work, the staff from the French Geological Survey (BRGM) office in Mayotte for providing logistical support during the MT survey, and the RÃ©seau de Surveillance Volcanologique et Sismologique de Mayotte (REVOSIMA) for coordinating the geoscientific efforts during the seismovolcanic crisis. The French Hydrographic Office (SHOM) provided the bathymetry used in the MT inversion. Data are available on the data repository 4TU.Centre for Research Data (https://doi.org/10.4121/uuid:cb760562-3d5f-43fd-b2b1-1612894ab0ec).

References

Abdelfettah, Y., Sailhac, P., Larnier, H., Matthey, P.D., Schill, E., 2018. Continuous and time-lapse magnetotelluric monitoring of low volume injection at rittershoffen geothermal project, northern alsace–france. Geothermics 71, 1–11.

Aizawa, K., Koyama, T., Uyeshima, M., Hase, H., Hashimoto, T., Kanda, W., Yoshimura, R., Utsugi, M., Ogawa, Y., Yamazaki, K., 2013. Magnetotelluric and temperature monitoring after the 2011 sub-plinian eruptions of shinmoe-dake volcano. Earth, Planets and Space 65, 6.

Audru, J.C., Bitri, A., Desprats, J.F., Dominique, P., Eucher, G., Hachim, S., Jossot, O., Mathon, C., Nédellec, J.L., Sabourault, P., et al., 2010. Major natural hazards in a tropical volcanic island: a review for mayotte island, comoros archipelago, indian ocean. Engineering geology 114, 364–381.

Baba, K., Chave, A.D., Evans, R.L., Hirth, G., Mackie, R.L., 2006. Mantle dynamics beneath the east pacific rise at 17 s: Insights from the mantle electromagnetic and tomography (melt) experiment. Journal of Geophysical Research: Solid Earth 111.

Booker, J.R., 2014. The magnetotelluric phase tensor: a critical review. Surveys in Geophysics 35, 7–40.

Cesca, S., Letort, J., Razafindrakoto, H.a., 2020. Drainage of a deep magma reservoir near mayotte inferred from seismicity and deformation. Nature Geoscience 13, 87–93.

Chave, A.D., Jones, A.G., 2012. The magnetotelluric method: Theory and practice. Cambridge University Press.

Chave, A.D., Thomson, D.J., 2004. Bounded influence magnetotelluric response function estimation. Geophysical Journal International 157, 988–1006.

Debeuf, D., 2004. Étude de l'évolution volcano-structurale et magmatique de mayotte (archipel des comores, océan indien). Université de la Reunion, 277.

Egbert, G.D., 2002. Processing and interpretation of electromagnetic induction array data. Surveys in geophysics 23, 207–249.

Emerick, C., Duncan, R., 1982. Age progressive volcanism in the comores archipelago, western indian ocean and implications for somali plate tectonics. Earth and Planetary Science Letters 60, 415–428.

Flóvenz, Ó., Spangenberg, E., Kulenkampff, J., Árnason, K., Karlsdóttir, R., Huenges, E., 2005.

The role of electrical interface conduction in geothermal exploration, in: Proceedings of the 2005 world geothermal congress, pp. 24–29.

Hautot, S., Single, R., Watson, J., Harrop, N., Jerram, D., Tarits, P., Whaler, K., Dawes, D., 2007. 3-d magnetotelluric inversion and model validation with gravity data for the investigation of flood basalts and associated volcanic rifted margins. Geophysical Journal International 170, 1418–1430.

Hautot, S., Tarits, P., Whaler, K., Le Gall, B., Tiercelin, J.J., Le Turdu, C., 2000. Deep structure of the baringo rift basin (central kenya) from three-dimensional magnetotelluric imaging: Implications for rift evolution. Journal of Geophysical Research: Solid Earth 105, 23493–23518.

Ingham, M., Bibby, H., Heise, W., Jones, K., Cairns, P., Dravitzki, S., Bennie, S., Caldwell, T., Ogawa, Y., 2009. A magnetotelluric study of mount ruapehu volcano, new zealand. Geophysical Journal International 179, 887–904

Junge, A., 1996. Characterization of and correction for cultural noise. Surveys in Geophysics 17, 361–391.

Kummerow, J., Raab, S., 2015 a. Temperature dependence of electrical resistivity–part ii: A new experimental set-up to study fluid saturated rocks. Energy Procedia 76, 247–255.

Kummerow, J., Raab, S., 2015 b. Temperature dependence of electrical resistivity-part i: Experimental investigations of hydrothermal fluids. Energy Procedia 76, 240–246.

Ladanivskyy, B., Zlotnicki, J., Revil, P., Alanis, P., 2018. Electromagnetic signals on active volcanoes: Analysis of electrical resistivity and transfer functions at taal volcano (philippines) related to the 2010 seismovolcanic crisis. Journal of Applied Geophysics 156, 67–81.

Laumonier, M., Farla, R., Frost, D.J., Katsura, T., Marquardt, K., Bouvier, A.S., Baumgartner, L.P., 2017. Experimental determination of melt interconnectivity and electrical conductivity in the upper mantle. Earth and Planetary Science Letters 463, 286–297.

Lemoine, A., Bertil, D., Roullé, A., Briole, P., 2019. The volcano-tectonic crisis of 2018 east of mayotte, comoros islands.

Michon, L., 2016. The volcanism of the comoros archipelago integrated at a regional scale, in: Active volcanoes of the southwest Indian Ocean. Springer, pp. 333–344.

Nono, F., Gibert, B., Parat, F., Loggia, D., Cichy, S.B., Violay, M., 2018. Electrical conductivity

of icelandic deep geothermal reservoirs up to supercritical conditions: Insight from laboratory experiments. Journal of Volcanology and Geothermal Research.

Nougier, J., Cantagrel, J., Karche, J., 1986. The comores archipelago in the western indian ocean: volcanology, geochronology and geodynamic setting. Journal of African Earth Sciences 5, 135–145.

Revil, A., Cathles, L., Losh, S., Nunn, J., 1998. Electrical conductivity in shaly sands with geophysical applications. Journal of Geophysical Research: Solid Earth 103, 23925–23936.

Saemundsson, K., Axelsson, G., Steingrmsson, B., 2009. Geothermal systems in global perspective. Short Course on Exploration for Geothermal Resources, UNU GTP 11.

Smai, F., Wawrzyniak, P., 2020. Razorback, an open source python library for robust processing of magnetotelluric data. Front. Earth Sci 8, 296.

Spichak, V., Manzella, A., 2009. Electromagnetic sounding of geothermal zones. Journal of Applied Geophysics 68, 459–478.

Ussher, G., Harvey, C., Johnstone, R., Anderson, E., 2000. Understanding the resistivities observed in geothermal systems, in: proceedings world geothermal congress, Kyushu. pp. 1915–1920.

Wawrzyniak, P., Zlotnicki, J., Sailhac, P., Marquis, G., 2017. Resistivity variations related to the large march 9, 1998 eruption at la fournaise volcano inferred by continuous mt monitoring. Journal of Volcanology and Geothermal Research.

Figure 1: **Left: geodynamic context of the Mayotte island, after Lemoine et al. (2019). Right: location of the MT stations deployed onshore and offshore Petite Terre island. The blue triangles represent the MT sites. The green circles represent the epicenters of the seismic events recorded from May 2018 to May 2019, after Lemoine et al. (2019). The red ellipses with an arrow represent the phase tensor ellipses at 1000 s at sites L0 and L2. Profile AA' is the location of the cross-section through the 3D resistivity model in Figure 4.**

Figure 2: **MT soundings for sites L2 (left panel) and M2 (right panel). The upper and lower panels display the apparent resistivity in $\Omega.m$ and phase in degrees, respectively. The full lines signify the responses of the best-fitting model.**

Figure 3: **Site L2. Four-day time-lapse remote reference processing results between May 29^{th} and June 28^{th}. (a) Three-hour Kp index, (b) phase tensor ellipses filled with the determinant apparent resistivity on a log$_{10}$ scale, and (c) successive 4-day interval estimates of the apparent resistivity components xy (upper left) and yx (upper right) and phase components xy (lower left) and yx (lower right).**

Figure 4: **N120° cross-section through the 3D resistivity volume obtained from the inversion of the land and marine MT data. Green circles represent the hypocenters of the seismic events recorded from May 1, 2018, to May 28, 2019 (Lemoine et al., 2019). Yellow triangles represent the MT sites used in the MT inversion.**

Figure 5: **Variation of the misfit between the tested and preferred model as a function of a) the resistivity of the deep conductive layer, b) the depth of the top of this conductor and c) the presence of a conductor between 5 and 13km depth to the South-East of Petite Terre. The value 0 corresponds to the preferred model.**

Figure 6: **Electrical resistivity structure of the Petite Terre island derived from inversion of the MT data and proposed interpretation of the geoelectric structure.**

Credit Authors
Darnet M.: supervision, funding acquisition, resources, investigation, writing original and review
Wawrzyniak P.: investigation, software, writing original and review
Tarits P.: investigation, software, resources, writing original and review
Hautot P.: investigation, software, writing original and review
D'Eu J.F.: investigation, resources, software

Declaration of interests

☒ The authors declare that they have no known competing financial interests or personal relationships that could have appeared to influence the work reported in this paper.

☐The authors declare the following financial interests/personal relationships which may be considered as potential competing interests:

Highlights

- A major seismovolcanic crisis has afflicted the islands of Mayotte, Comoros Archipelago, since May 2018, although the origin is debated.
- We report the results of a preliminary land and shallow marine MT survey performed on and offshore the island nearest the crisis.
- The 3D inversion-derived electrical resistivity model suggests that the island is underlain by a shallow ~500-m-thick conductive layer atop a deeper, more resistive layer, possibly associated with a high-temperature geothermal system.
- At depths of ~15 km, the resistivity drops by almost two orders of magnitude, possibly due to partial melting.

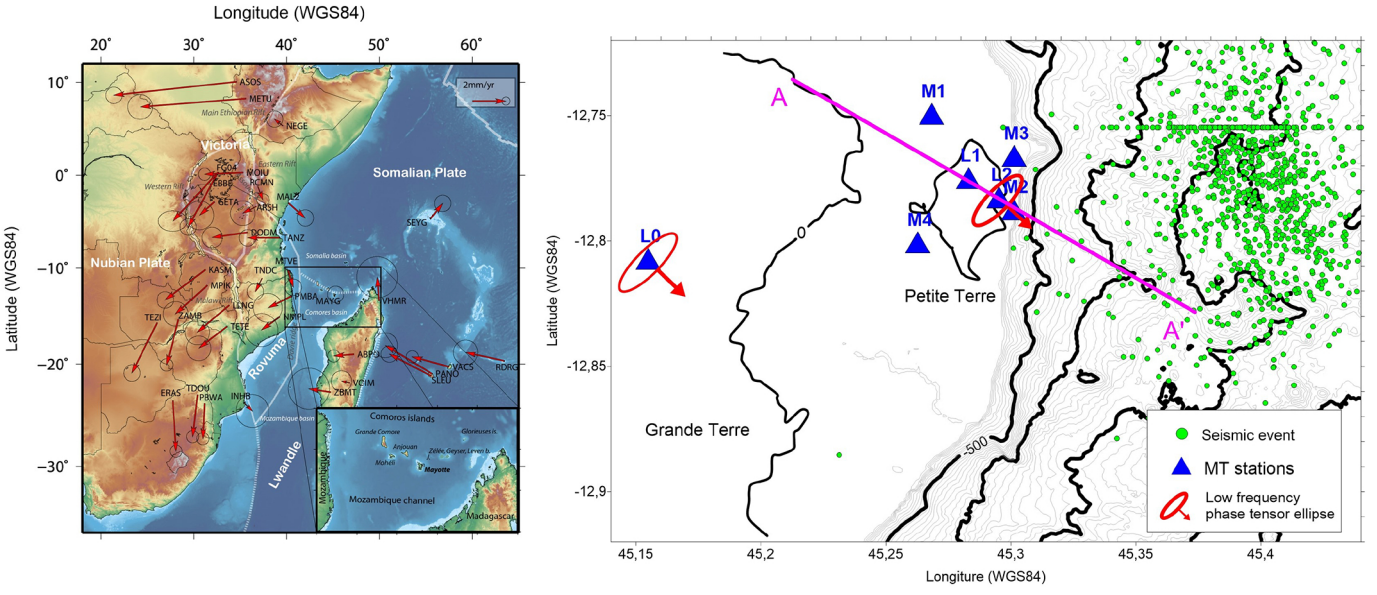
Longitude (WGS84)
Latitude (WGS84)
20°
30°
40°
50°
60°
10°
0°
−10°
−20°
−30°
2mm/yr
Victoria
Somalian Plate
Nubian Plate
Rovuma
Lwandile
Somalia basin
Mozambique basin
Mozambique channel
Madagascar
Comoros islands
Grande Comore
Anjouan
Mohéli
Mayotte
Gloreuses is.
ASOS
METU
NEGE
FCO4
KONJ
EBRE
RCMN
SETA
MALI
ARSH
SEYG
DODM
TANZ
MTVE
KASM
TNDC
MPIK
PMBA
MAYG
LLNG
NRTL
VHMR
TEZI
ZAMB
TETE
ABPS
CVACS
PANO
SLEU
RDRG
VEIM
ZBMT
ERAS
TDOU
PRWA
INHB
A
A'
M1
M2
M3
M4
L1
L2
L0
0
-500
Petite Terre
Grande Terre
-12,75
-12,8
-12,85
-12,9
45,15
45,2
45,25
45,3
45,35
45,4
Longitude (WGS84)
Seismic event
MT stations
Low frequency
phase tensor ellipse

Figure 1

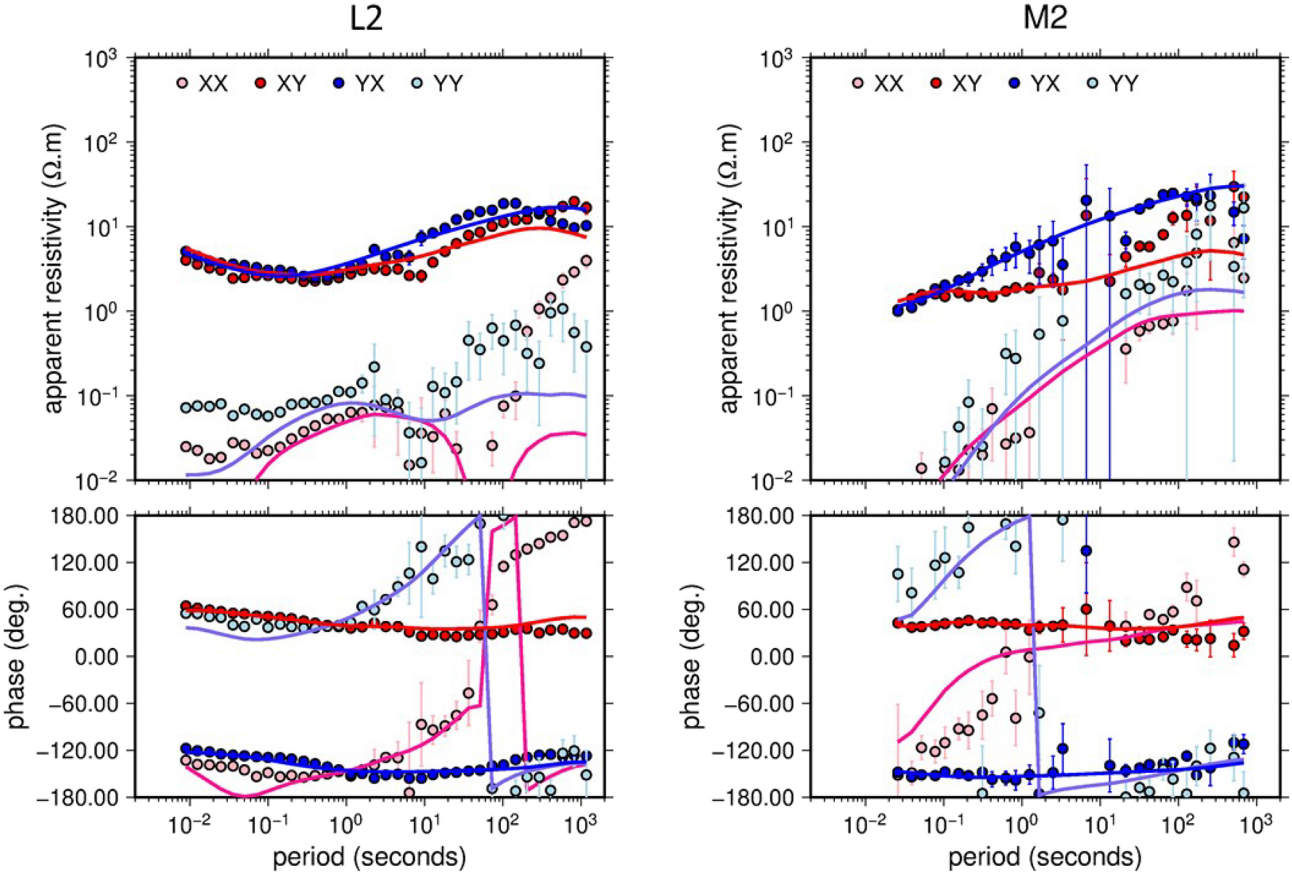
L2
M2
XX
XY
YX
YY
apparent resistivity (Ω.m)
phase (deg.)
period (seconds)

Figure 2

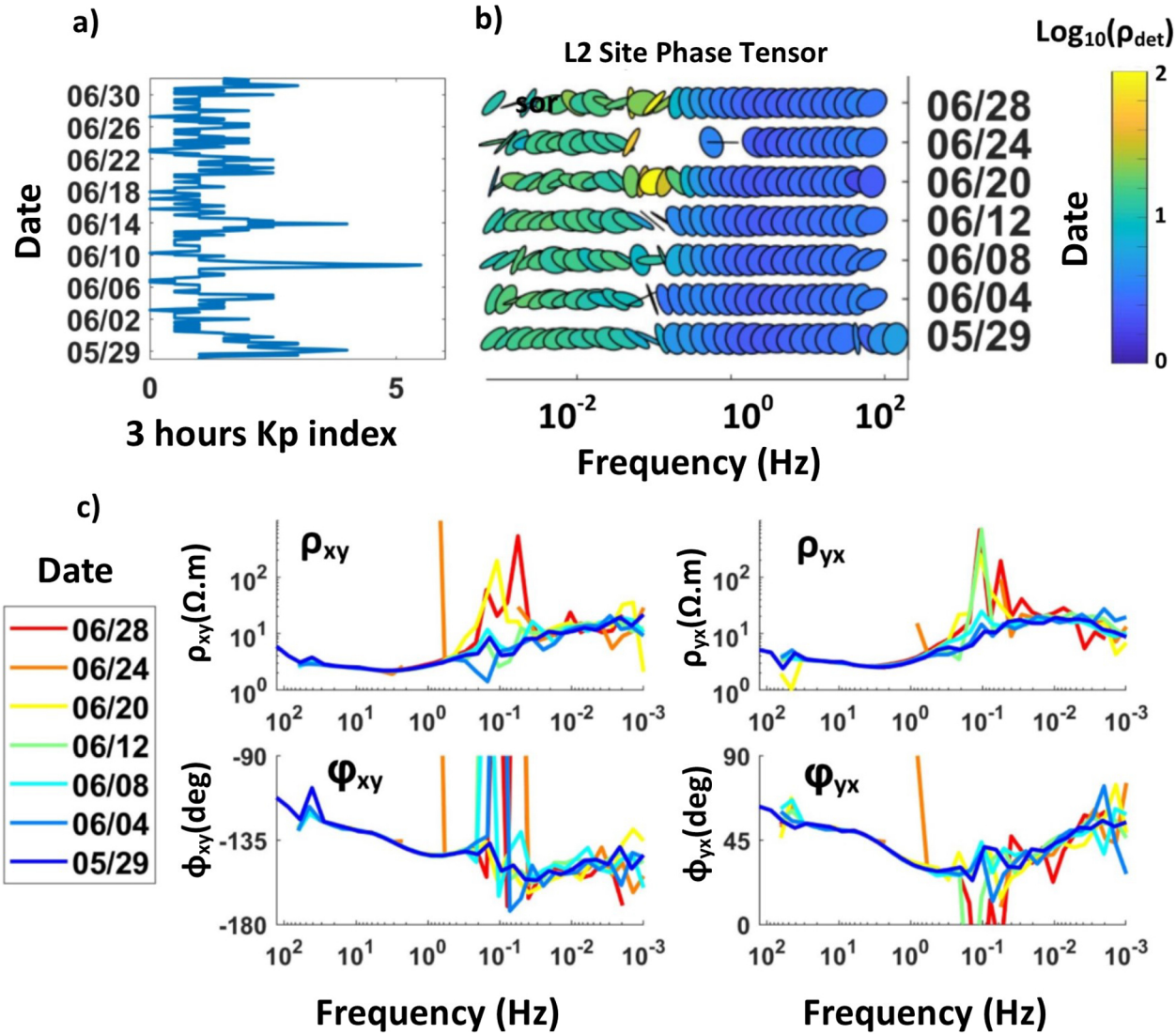
a)
Date
06/30
06/26
06/22
06/18
06/14
06/10
06/06
06/02
05/29
0
5
3 hours Kp index
b)
L2 Site Phase Tensor
Log10(ρdet)
2
1
0
Date
06/28
06/24
06/20
06/12
06/08
06/04
05/29
10-2
100
102
Frequency (Hz)
c)
Date
06/28
06/24
06/20
06/12
06/08
06/04
05/29
ρxy
ρxy(Ω.m)
ρyx
ρyx(Ω.m)
φxy
φxy(deg)
φyx
φyx(deg)
-90
-135
-180
90
45
0
Frequency (Hz)
Frequency (Hz)

Figure 3

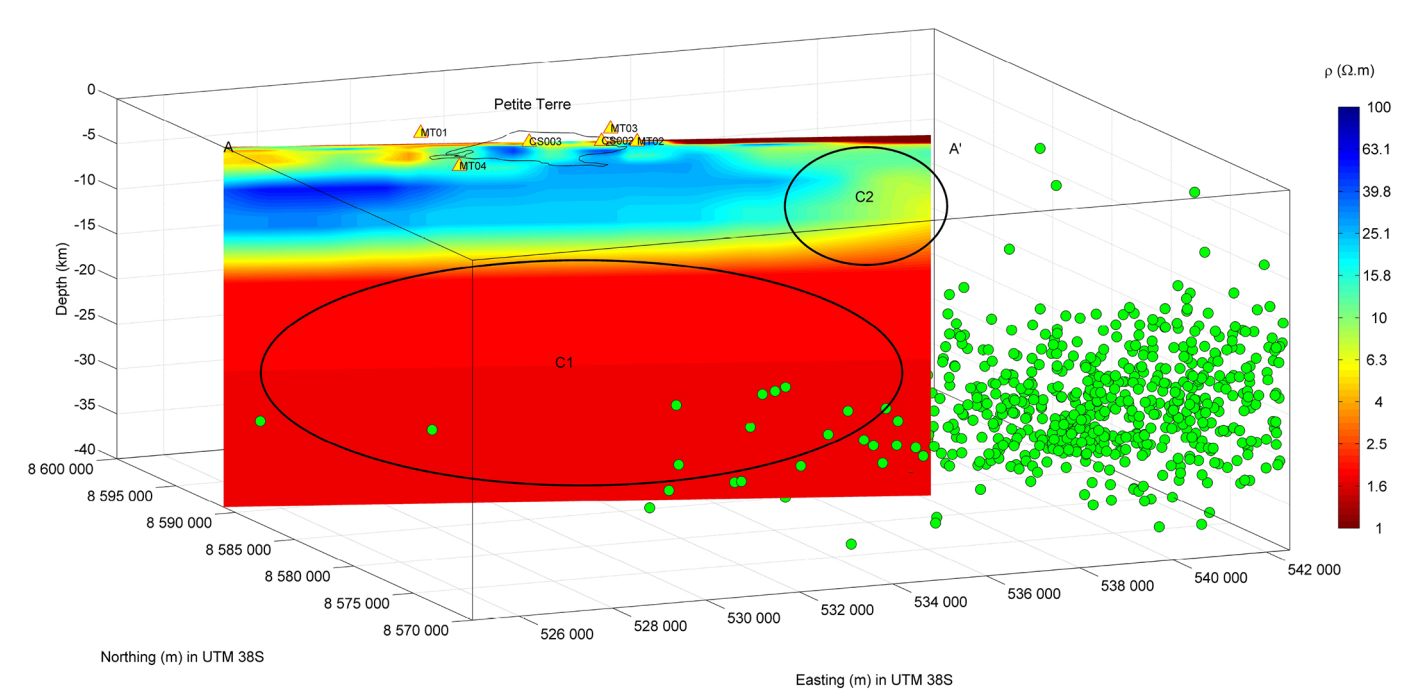
Petite Terre
MT01
MT03
CS003
CS002
MT02
MT04
A
A'
C1
C2
Depth (km)
0
-5
-10
-15
-20
-25
-30
-35
-40
ρ (Ω.m)
100
63.1
39.8
25.1
15.8
10
6.3
4
2.5
1.6
1
8 600 000
8 595 000
8 590 000
8 585 000
8 580 000
8 575 000
8 570 000
Northing (m) in UTM 38S
526 000
528 000
530 000
532 000
534 000
536 000
538 000
540 000
542 000
Easting (m) in UTM 38S

Figure 4

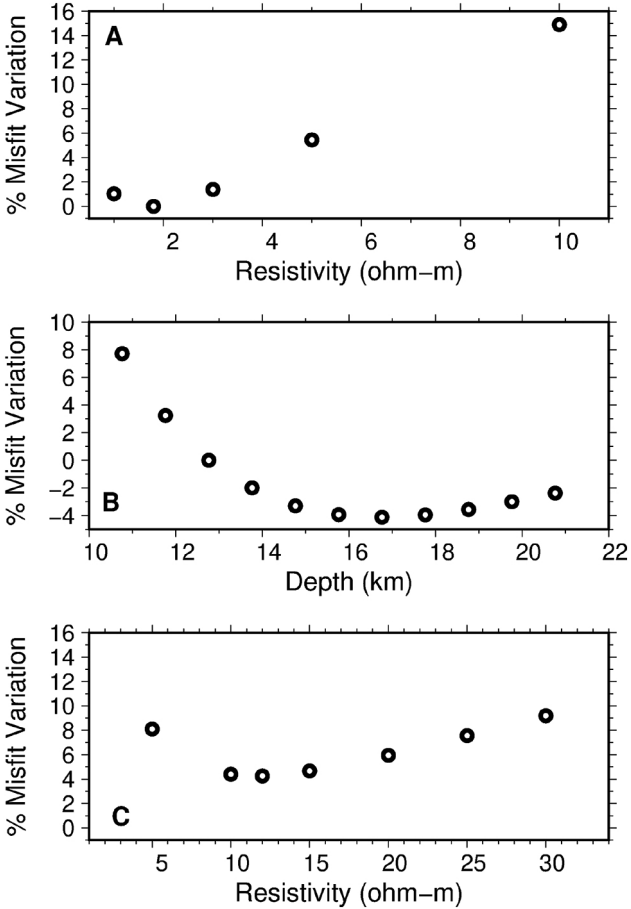
A
% Misfit Variation
Resistivity (ohm–m)
B
% Misfit Variation
Depth (km)
C
% Misfit Variation
Resistivity (ohm–m)

Figure 5

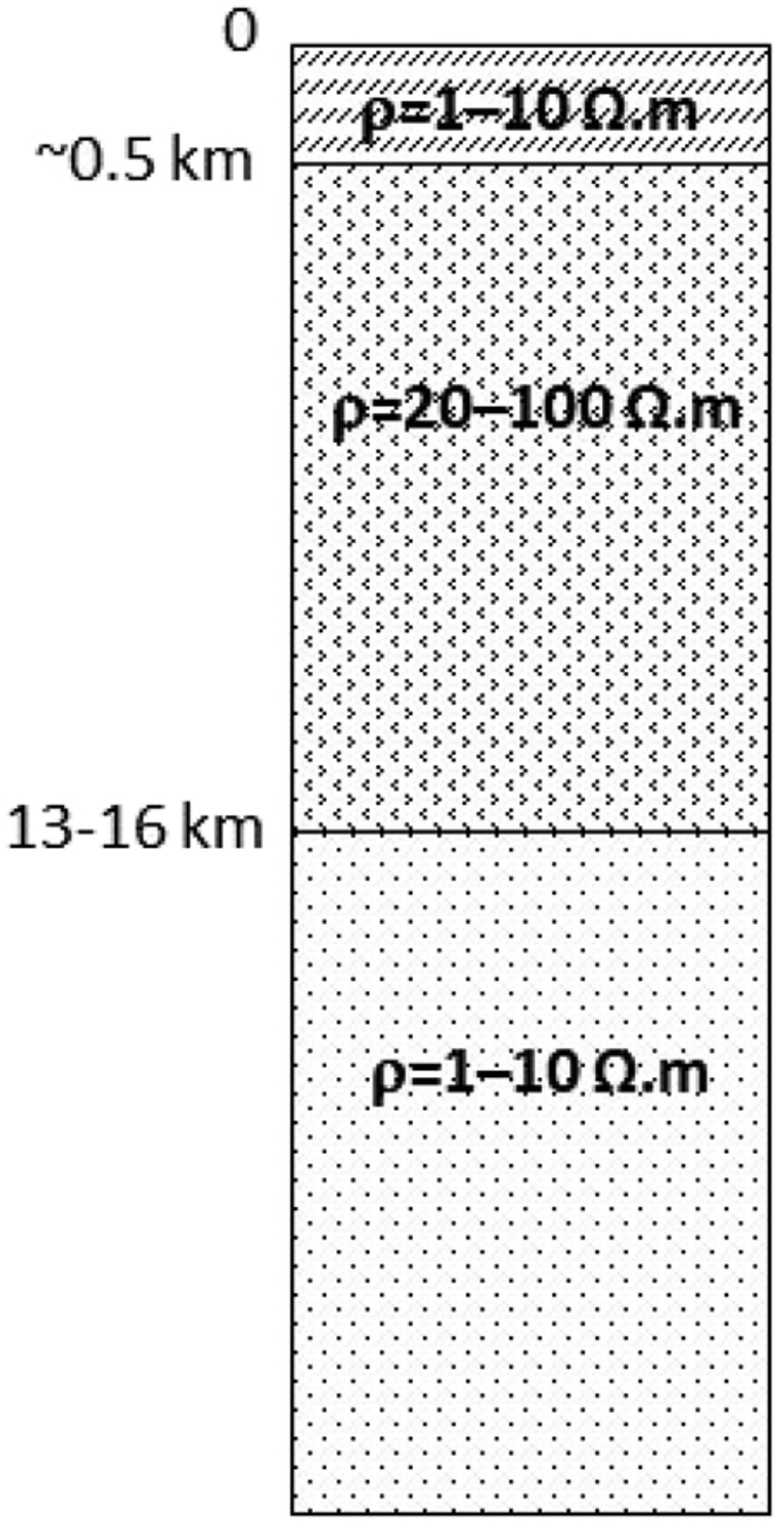

Smectite-rich, low-temperature (<220◦C), hydrothermally altered layer (clay cap)

Illite-rich, high-temperature (>220◦C), hydrothermally altered layer (geothermal reservoir?) then low porosity material (crust)

Presence of melt?

Figure 6